Journal of Solid State Chemistry **152,** 503–510 (2000)
doi:10.1006/jssc.2000.8719, available online at http://www.idealibrary.com on IDEAL®

Structural and Magnetic Properties of Ultrafine $La_{0.7}Ca_{0.3}MnO_z$ Powders Prepared by Mechanical Alloying

M. Muroi,[1] R. Street, and P. G. McCormick

Special Research Centre for Advanced Mineral and Materials Processing, Department of Physics, The University of Western Australia, Nedlands, WA 6907 Australia

Received November 17, 1999; in revised form March 8, 2000; accepted March 16, 2000

Ultrafine $La_{0.7}Ca_{0.3}MnO_z$ powders with controlled oxygen stoichiometry have been synthesized by mechanical alloying at ambient temperature. It is found that high-energy ball milling of the starting materials, La_2O_3, CaO, MnO_2, and Mn_3O_4 mixed in the stoichiometric cation ratio, yields single-phase $La_{0.7}Ca_{0.3}MnO_z$ powders having crystallite sizes of about 10 nm and various oxygen content ($2.68 \le z \le 3.35$), adjustable by changing the MnO_2/Mn_3O_4 ratio. Magnetic measurements show that the spontaneous magnetization (M_s) of the as-milled powder depends less on the nominal Mn valence (v_{Mn}) than in bulk (La, Ca)MnO_3 and that the maximum M_s, observed for $v_{Mn} \sim 3.3$, is much smaller. Annealing in air at temperatures above 500°C increases M_s for all the samples, but a marked increase in M_s toward the bulk value ($\sim$90 emu/g) occurs in a lower temperature range for lower v_{Mn} than for higher v_{Mn}. These observations are discussed in terms of magnetic disorder resulting from defects induced by high-energy milling and surface effects dominant in small crystals. © 2000 Academic Press

INTRODUCTION

Mixed-valence manganites of the type $R_{1-x}A_xMnO_3$, where R is a rare-earth element and A is an alkali-earth element, have been the subject of intense research for more than half a century from both scientific and technological viewpoints (1–29). On the one hand, they exhibit a variety of unique properties, such as an insulator–metal transition that accompanies a ferromagnetic transition (1), the colossal magnetoresistance effect (1,2), field-induced structural changes (3), and high catalytic activity (4); it is of fundamental importance to elucidate the underlying mechanisms responsible for these phenomena. On the other hand, mixed-valence manganites have vast potential for use in a wide range of applications; for example, they can be used as the materials for magnetic recording heads and sensors (5), cathode materials in solid oxide fuel cells (6), working substances of magnetic refrigerators (7), and catalysts (4).

$R_{1-x}A_xMnO_3$, having the perovskite structure, can be synthesized by various methods. The most widely used is standard ceramic processing, or solid-state reaction between oxides carbonates, hydroxides, etc., of the constituent cations. Despite its simplicity, this method has the disadvantage that repeated cycles of calcining and grinding at high temperatures, typically above 1000°C, are necessary to obtain homogeneous single-phase materials. This problem is greatly alleviated in wet-chemical methods, in which a precursor gel is prepared by co-precipitation (8). Since the constituent cations in the precursor are intimately mixed as poorly crystallized hydroxides, the $R_{1-x}A_xMnO_3$ phase is formed at relatively low temperatures (540–700°C). The crystallite size of the resultant powder could thus be made very small, down to 20 nm, which, on the one hand, allows low-temperature sintering and, on the other, is favorable in some applications such as catalysts. Drawbacks of this method include low yield and the necessity of a prefiring step to remove organic compounds. As an alternative to wet-chemical methods, mechanical alloying has recently been applied to the synthesis of $La_{0.7}Sr_{0.06}Ca_{0.24}MnO_3$ powders (9). In this method, high-energy ball milling is used to prepare an amorphous mixture of carbonates and hydroxides. The process, however, involves milling for a prolonged time of over 100 h and still requires post-milling heat treatment at a temperature of above 700°C to form the perovskite phase. Other synthesis methods include thin film deposition (10) and single-crystal growth (1–3), in which $R_{1-x}A_xMnO_3$ crystals grow directly from gas or liquid phases. Because of the high cost and low yield, however, these techniques are currently used mainly for research purposes, and their application will be limited to special areas such as microelectronics.

In this work, we have succeeded in synthesizing ultrafine powders of $La_{0.7}Ca_{0.3}MnO_z$, a representative mixed-valence manganite, by the simplest possible process: *single-step milling of constituent oxides at ambient temperature*. It is

[1]To whom correspondence should be addressed. E-mail: muroi@physics.uwa.edu.au.

0022-4596/00 $35.00

shown that single-phase $La_{0.7}Ca_{0.3}MnO_z$ powders having crystallite sizes of about 10 nm are obtained by high-energy ball milling for only 5 h, and furthermore the oxygen stoichiometry (z) can be controlled simply by adjusting the oxygen content of the starting materials. The results of an extensive study of the magnetic properties of the as-milled powders, and of the effects of annealing, are also presented and discussed.

EXPERIMENTAL PROCEDURES

$La_{0.7}Ca_{0.3}MnO_z$ powders were prepared by mechanical alloying. The starting materials used were La_2O_3, CaO, MnO_2, and Mn_3O_4 mixed in the ratio appropriate for the reaction

$$0.35La_2O_3 + 0.3CaO + (1 - x)MnO_2 + (x/3)Mn_3O_4 \rightarrow La_{0.7}Ca_{0.3}MnO_{3.35-(2/3)x}. \quad [1]$$

A total of 4 g of the starting powder, together with seven hardened-steel balls 12.7 mm in diameter, was loaded into a hardened-steel vial in an Ar-filled glovebox and milled for 5 h in a SPEX 8000 mixer/mill. Five batches of powders were prepared, as listed in Table 1, where the mixing ratio of the manganese oxides (x), the expected oxygen stoichiometry (z), and the nominal Mn valence (v_{Mn}) are indicated. (In the following, we use v_{Mn} to specify the samples.) The milled powders were annealed in air at temperatures between 500 and 1450°C. The annealing time was kept at 30 min except for the annealing temperature (T_a) of 1450°C, at which the powders were annealed for 12 h to obtained micrometer-size crystals. The crystal structure of the powders was determined by X-ray diffraction (XRD), and the morphology was examined by transmission electron microscopy (TEM) or scanning electron microscopy (SEM). The oxygen content of the as-milled powders was analyzed by combustimetry as well as thermogravimetry (TG). Magnetic measurements were made on cold-pressed pellets 5 mm in diameter and about 1 mm thick using a SQUID magnetometer. The magnetic field was applied parallel to the flat surfaces of the pellet to reduce demagnetization effects.

TABLE 1
Mixing Ratio of Manganese Oxides in the Starting Material (x in Reaction 1), Nominal Oxygen Stoichiometry (z), and Nominal Mn Valence (v_{Mn}) for Five Samples Prepared

Sample no.	x in reaction 1	z	v_{Mn}
1	0	3.350	4.000
2	0.3	3.150	3.600
3	0.525	3.000	3.300
4	0.75	2.850	3.000
5	1	2.683	2.667

RESULTS AND DISCUSSION

1. Crystal Structure and Oxygen Stoichiometry

In Fig. 1, XRD spectra for the as-milled powders are shown. All the peaks correspond to the cubic perovskite structure, indicating that reaction [1] was essentially completed during milling. (We attempted to prepare powders having v_{Mn} lower than 2.67 by using MnO and Mn_3O_4 as the source of Mn, which resulted in multiphase powders.) The crystallite size (D), estimated from XRD peak broadening using Scherrer's formula, is in the range 8–13 nm and tends to become smaller as v_{Mn} deviates from 3.3, as can be seen in the inset of Fig. 2a, where D is plotted as a function of v_{Mn}.

TEM photographs of the as-milled powder with $v_{Mn} = 3.3$ are shown in Fig. 3. It can be seen that the powder consists of heavily agglomerated crystallites ranging between about 5 and 20 nm in size, consistent with the crystallite size determined from XRD peak broadening, 13 nm. Similar microstructures were observed for the other as-milled powders having different values of v_{Mn}. The v_{Mn} dependence of D (inset of Fig. 2a) could not be confirmed, however, because of the heavy agglomeration and the relatively broad distribution of D, which made quantitative evaluation of D difficult. Furthermore, the difference in the degree of XRD peak broadening could also arise from the difference in the density of defects, as discussed later.

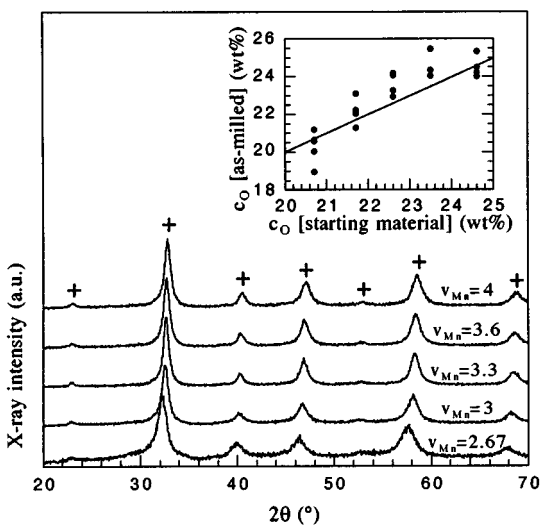

FIG. 1. XRD spectra for the as-milled powders with various values of v_{Mn}. Crosses (+) indicate peaks corresponding to the perovskite phase. Inset: Oxygen content (c_O) of the as-milled powder plotted as a function of c_O of the starting material. The c_O of the as-milled powders was determined by combustimetry. At least four measurements were made for each v_{Mn}, and all data are plotted.

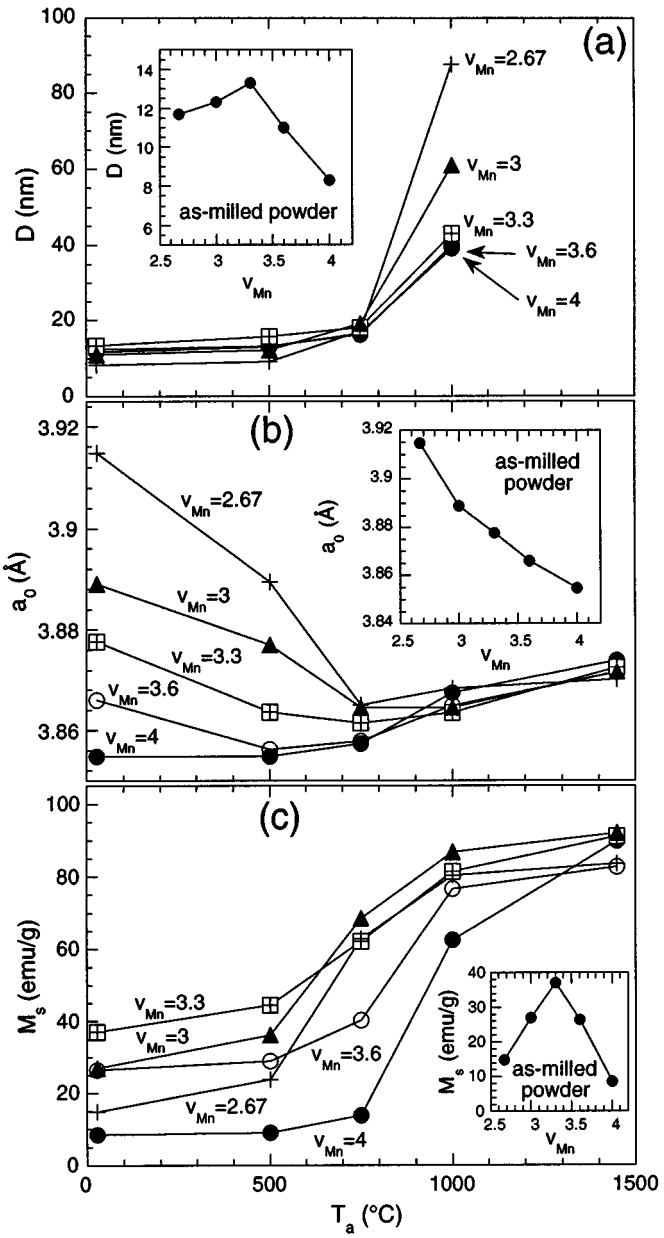

FIG. 2. Variations with annealing temperature, T_a, of (a) the crystallite size, D, (b) the lattice constant, a_0, and (c) the spontaneous magnetization, M_s, for the powders with various values of v_{Mn}. The insets show the v_{Mn} dependence of D, a_0, and M_s for the as-milled powders.

In the inset of Fig. 1, the oxygen content (c_O) of the as-milled powder, determined by combustimetry, is plotted as a function of c_O of the starting material. The data clearly show that the as-milled powders have approximately the same c_O as the starting mixtures.

The variations of D with T_a are shown in Fig. 2a. Regardless of v_{Mn}, D increases with T_a, very slowly below 750°C and at an accelerated rate above 750°C. A similar feature has been observed for $La_{0.7}Ca_{0.3}MnO_3$ powders prepared by the sol–gel method (8). SEM examination has confirmed that the grain size of the powders annealed at 1450°C is a few micrometers and has no apparent correlation with v_{Mn}.

In the inset of Fig. 2b, the lattice constant (a_0) of the as-milled powder, determined from the XRD data on the basis of cubic symmetry, is plotted as a function of v_{Mn}. It can be seen that a_0 decreases with increasing v_{Mn}, as expected from the decrease in the ionic size of Mn with increasing oxidation state.

The TG curves for the as-milled powders are shown in Fig. 4. The five curves are assembled so that they merge in the temperature range 1400–1500°C, where they have similar slopes, and, therefore, the five samples are expected to have the same equilibrium oxygen stoichiometry. The sample mass at 1450°C is taken as the reference, and the relative mass change (left vertical axis) is converted to the relative change in the oxygen content Δz (right vertical axis) on the basis of the chemical formula $La_{0.7}Ca_{0.3}MnO_z$. The separation between the TG curves at low temperature ($< \sim 300$°C) is in reasonable agreement with the expected difference in z (Table 1), demonstrating further that the oxygen content of the as-milled powders reflects that of the starting materials. The mass increase below 500°C for $v_{Mn} = 3$ and 2.67 roughly corresponds to the oxygen deficiency $(3 - z)$ and is ascribed to the filling of oxygen vacancies, while the mass decrease in the range 700–1400°C, which is larger the higher v_{Mn}, is considered to result from the release of O_2 that accompanies the filling of cation vacancies[2]; it is well known that in perovskite manganites excess oxygen atoms are accommodated by forming cation vacancies (11, 12). (The mass decrease below ~ 500°C is due to the release of adsorbed water, which was verified by analyzing the released gas using a mass spectrometer.)

The variations of a_0 with T_a are plotted in Fig. 2b. After annealing at 1450°C, a_0 converges in a narrow range, 3.870–3.874 Å; these values are similar to a_0 of bulk $La_{0.7}Ca_{0.3}MnO_3$ (13). The overall changes in a_0 upon annealing are consistent with the oxygen stoichiometry of the as-milled powders. For $v_{Mn} \leq 3$, the as-milled powders are oxygen-deficient ($z < 3$), and the oxygen vacancies are filled during annealing, resulting in an increase in the Mn oxidation state and hence a decrease in a_0. For $v_{Mn} \geq 3.6$, on the other hand, the as-milled powders have excess oxygen

[2]The higher temperature required for filling cation vacancies, as compared with that required for filling oxygen vacancies, seems reasonable in view of the perovskite structure. In $La_{0.7}Ca_{0.3}MnO_z$ the ionic size of La^{3+} and Ca^{2+} is comparable to that of O^{2-}, but the nearest-neighbor separation is much larger for the La/Ca site (a_0) than for the O site ($a_0/2^{1/2}$), making the diffusion of the former more difficult. The smaller Mn ions would be able to diffuse more easily, but preservation of uniform composition requires that La/Ca and Mn ions diffuse simultaneously; that is, the filling of cation vacancies is limited by the slower La/Ca diffusion.

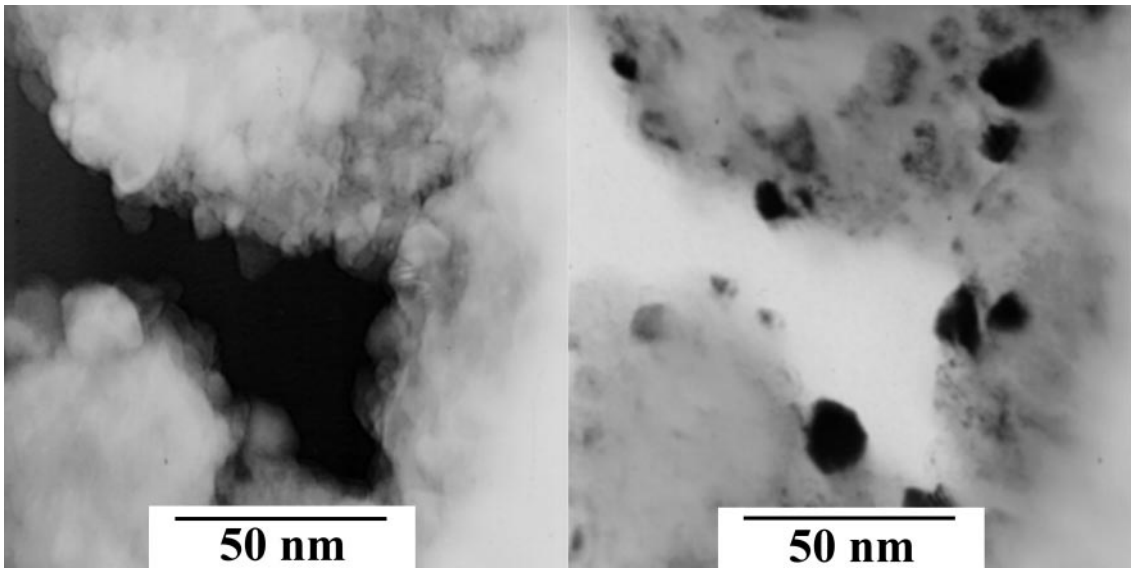

FIG. 3. TEM photographs of the as-milled powder with $v_{Mn} = 3.3$ (left, bright-field image; right, dark-field image).

atoms ($z > 3$), which are accommodated by forming cation vacancies (11, 12). Upon annealing, the cation vacancies are filled, resulting in a decrease in the Mn oxidation state and hence an increase in a_0. For $v_{Mn} \leq 3.6$, however, the variations of a_0 as a function of T_a are not monotonic, exhibiting minima in the temperature range 500–750°C. This is explained by assuming the presence of Schottky-type defects induced by high-energy ball milling, in addition to the intrinsic defects due to oxygen nonstoichiometry. For instance, the powder with $v_{Mn} = 3.3$ is stoichiometric ($z = 3$), but it could contain vacancies on both the cation and oxygen sites. (From the stoichiometry, the cation and oxygen vacancies must be in the ratio of 2 : 3.) Similarly, the nonstoichiometric samples ($v_{Mn} \neq 3.3$) may have vacancies on both the cation and oxygen sites, with the ratio of the former to the latter increasing with v_{Mn} (see below). Since the oxygen vacancies are filled in a lower temperature range ($< \sim 500$°C) than the cation vacancies ($> \sim 700$°C), as indicated by the TG data, the Mn oxidation state initially increases, resulting in a minimum in the a_0 versus T_a plot.

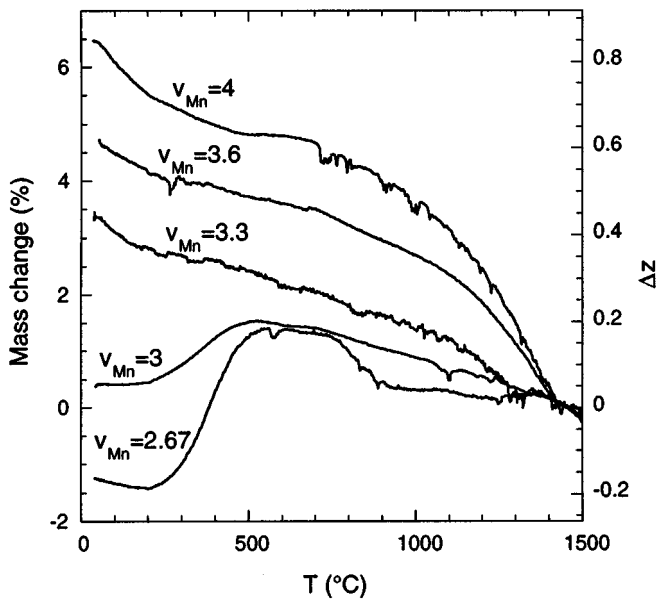

FIG. 4. TG curves for the as-milled powders having various values of v_{Mn}.

We can estimate the defect densities in the as-milled powders on the following assumptions: (i) cation vacancies are created on the La/Ca and Mn sites with an equal probability, and the chemical formula of the powders is expressed as $La_{0.7(1-\alpha)}Ca_{0.3(1-\alpha)}Mn_{1-\alpha}O_{3(1-\beta)}$; (ii) at T_a where a_0 has a minimum value, the oxygen sites are fully occupied, i.e., $z = 3$ ($\beta = 0$); and (iii) a_0 is a unique function of v_{Mn} represented by the a_0 versus v_{Mn} plot for the as-milled powders (inset, Fig. 2b). First, from assumption (iii), the average Mn valence of the powder having the minimum a_0, denoted as v^*_{Mn}, is determined using the a_0 versus v_{Mn} relationship (inset, Fig. 2b). Then, α is obtained from the charge neutrality condition for the powder with the minimum a_0, $2.7(1-\alpha) + v^*_{Mn}(1-\alpha) - 6 = 0$ ($\beta = 0$ from assumption (ii)). Finally, the charge neutrality condition for the as-milled powder, $2.7(1-\alpha) + v_{Mn}(1-\alpha) - 6(1-\beta) = 0$, is used to determine the values of β. The defect densities, α and β, thus obtained are plotted as functions of v_{Mn} in Fig. 5; in the same graph, the densities of the intrinsic defects arising only from oxygen nonstoichiometry (without additional

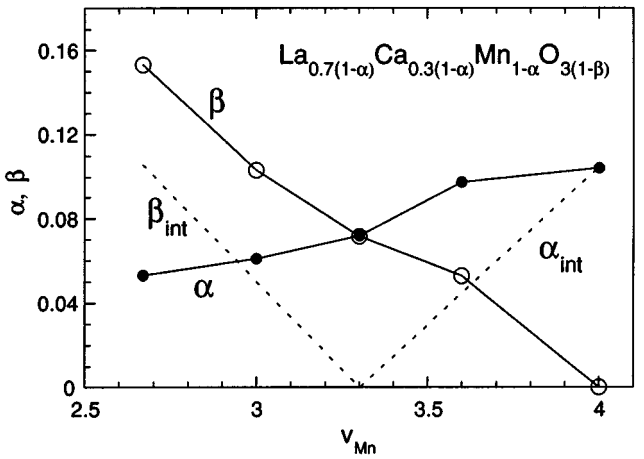

FIG. 5. Density of cation vacancies, α, and that of oxygen vacancies, β, plotted as functions of v_{Mn}. α and β were determined from the a_0 versus T_a plots (Fig. 2b) following the procedure described in the text. The densities of intrinsic vacancies arising only from oxygen nonstoichiometry, $\alpha_{int} = (v_{Mn} - 3.3)/(v_{Mn} + 2.7)$ and $\beta_{int} = 0.55 - v_{Mn}/6$, are indicated with dotted lines.

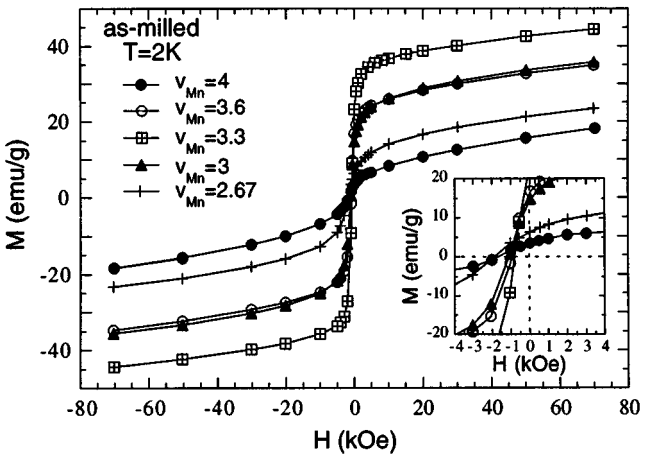

FIG. 6. Demagnetization curves at 2 K for the as-milled powders having various values of v_{Mn}. The plots in the low-field region are magnified in the insets.

Schottky-type defects), $\alpha_{int} = (v_{Mn} - 3.3)/(v_{Mn} + 2.7)$ and $\beta_{int} = 0.55 - v_{Mn}/6$, are also shown with dotted lines. It can be seen that α increases and β decreases as v_{Mn} increases, and that oxygen vacancies (cation vacancies) are the dominant defects for lower (higher) v_{Mn}, as expected. Except for $v_{Mn} = 4$, α and β are much greater than α_{int} and β_{int}, respectively, because of the additional Schottky-type defects. The enhanced defect densities seem to be reasonable, considering the nature of milling: it tends to increase the entropy of the system through mixing, thus favoring a phase with more defects and hence a larger entropy.

2. Magnetic Properties

In Fig. 6, the demagnetization curves for the as-milled powders measured at 2 K are displayed; details of the low-field region are shown in the inset. The following features are observed: (i) the spontaneous magnetization (M_s) is significantly smaller than the value for full alignment of the Mn spins, $M_{s,max} \sim 90$ emu/g (M_s is defined here as the value of magnetization obtained by linear extrapolation of the data points for $H \geq 30$ kOe to $H = 0$); (ii) the coercivities (H_c) are large, in the range 800–1800 Oe, and decrease quickly with increasing temperature, as can be seen in Fig. 7, where H_c is plotted as a function of temperature; and (iii) the magnetization does not saturate even at 70 kOe. These features, all characteristic of spin-glass systems (30), resemble those observed in radiation-damaged $La_{0.7}Ca_{0.3}MnO_3$ (10), Fe-doped (La, Ca)MnO_3 (14), and Co-doped (La, Sr)MnO_3 (15). M_s (H_c) is the largest (smallest) for $v_{Mn} = 3.3$ and decreases (increases) as v_{Mn} deviates from 3.3, suggesting that the sample with $v_{Mn} = 3.3$ is least disordered. The v_{Mn} dependence of M_s, shown in the inset of Fig. 2c, is much weaker than in bulk $La_{1-x}Ca_xMnO_3$ (11), although M_s still takes a maximum at $v_{Mn} \sim 3.3$; note that the as-milled powders with $v_{Mn} = 3$ and 3.6 have much *larger* M_s (26–27 emu/g) than bulk $La_{1-x}Ca_xMnO_3$ with $x = 0$ and 0.6 (< 0.5 emu/g (13)).

The temperature dependence of field-cooled magnetization ($H = 10$ kOe) is shown in Fig. 8 for various values of v_{Mn}. All the samples exhibit ferromagnetic transitions with T_c values in the range 100–200 K. (T_c is defined here as the temperature corresponding to the inflection point of the M versus T curve.) However, the transition is very broad, particularly for $v_{Mn} = 4$ and 2.67, indicating the presence of significant magnetic disorder. The

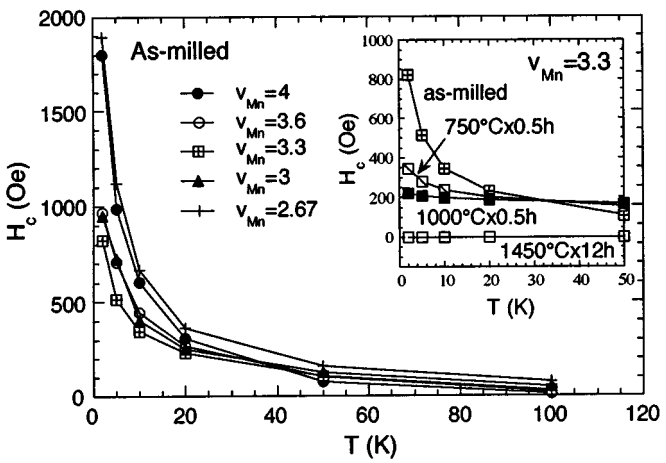

FIG. 7. Temperature dependence of coercivity (H_c) for the as-milled powders having various values of v_{Mn}. Inset: Temperature dependence of H_c for the powder with $v_{Mn} = 3.3$ (as-milled and annealed).

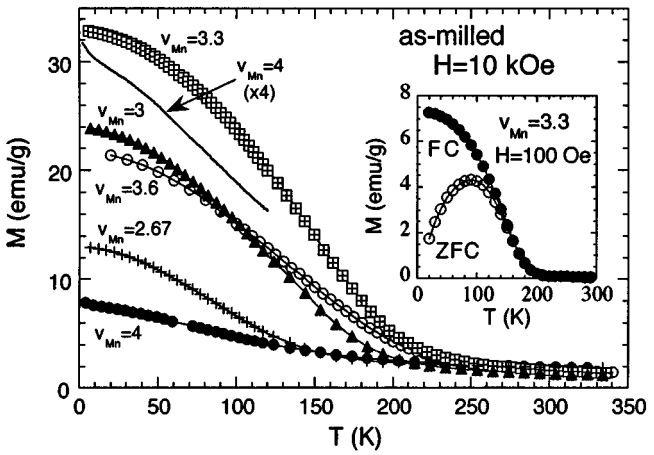

FIG. 8. Magnetization versus temperature plots for the as-milled powders having various values of v_{Mn}. The measurements were made in a field of 10 kOe. Inset: Magnetization versus temperature plots measured in a lower field of 100 Oe for the as-milled powder with $v_{Mn} = 3.3$. Both field-cooled and zero-field-cooled branches are shown.

magnetization at low temperature decreases as v_{Mn} deviates from 3.3, consistent with the variation M_s with v_{Mn} (inset, Fig. 2c).

In the inset of Fig. 8, the variations with temperature of the field-cooled (FC) and zero-field-cooled (ZFC) magnetizations ($H = 100$ Oe) are presented for $v_{Mn} = 3.3$. While the FC magnetization increases monotonically with decreasing temperature, the ZFC magnetization takes a maximum at ~ 90 K. This behavior is also characteristic of spin–glass systems, indicating again the presence of magnetic disorder.

The variations of M_s with annealing temperature (T_a) are shown in Fig. 2c. Regardless of v_{Mn}, M_s increases with T_a, reaching a value close to $M_{s,max}$ at $T_a = 1450°C$; however, the way M_s approaches $M_{s,max}$ depends on v_{Mn}. For higher v_{Mn} (4 and 3.6), M_s is essentially constant below 500°C and increases most rapidly in the range 750–1000°C. For lower v_{Mn} (3 and 2.67), on the other hand, M_s increases significantly even at 500°C, and a marked increase in M_s is observed in the range 500–750°C. The behavior for $v_{Mn} = 3.3$ is intermediate.

The effect of annealing on H_c for the powder with $v_{Mn} = 3.3$ is shown in the inset of Fig. 7. It can be seen that the temperature dependence of H_c becomes weaker as T_a increases. At $T_a = 1000°C$, H_c is about 200 Oe, almost independent of temperature, and at 1450°C, H_c becomes essentially zero (below the remanent field of the superconducting magnet used in the measurement, < 5 Oe) at all temperatures.

We discuss the magnetic properties described above in terms of competition between ferromagnetic (FM) and antiferromagnetic (AF) interactions, inherent in mixed-valence manganites[3]; double exchange (DE) interactions (16), mediated by e_g electrons delocalized among Mn ions in the mixed-valence state ($Mn^{3+/4+}$), are positive, whereas superexchange (SE) interactions, operative between Mn ions having a definite valence (Mn^{2+}, Mn^{3+}, and Mn^{4+}), can have either sign, depending on the valence of neighboring Mn ions and, when Mn^{3+} is involved, on whether or not static orbital ordering is present (31), as listed in Table 2. In bulk $La_{0.7}Ca_{0.3}MnO_3$ with no defects, DE interactions effected by delocalized e_g electrons are dominant throughout, and the material behaves as an essentially homogeneous ferromagnet. In the as-milled $La_{0.7}Ca_{0.3}MnO_3$ powder, global ferromagnetism is not realized because of the following two effects.

First, the random fluctuation of electrostatic potential due to the presence of vacancies tend to localize e_g electrons near the vacancies, thus turning part of the $Mn^{3+/4+}$ ions into Mn^{3+} and Mn^{4+} ions. [The effect of vacancies on the potential fluctuation is stronger than that of the divalent cations substituted for La, e.g., Ca ions in $La_{1-x}Ca_xMnO_3$, because of the higher effective charges of the former (17, 19, 20).] This results in an introduction of negative SE interactions between Mn^{4+} ions,[4] which tend to be trapped near cation vacancies (18). The coexistence of positive and negative exchange interactions causes frustration, resulting in a spin–glass state at low temperature (30). The electronic and magnetic structures in the as-milled $La_{0.7}Ca_{0.3}MnO_3$ powder are probably similar to those in $LaMnO_{3+\delta}$ ($\delta \sim 0.15$) which also has a v_{Mn} of 3.3, contains a high density of cation vacancies and exhibits magnetic properties very similar to those of the former (17, 18, 23). The coexistence of

[3]As an inevitable consequence of high-energy milling using a steel vial and grinding media, the as-milled powders contained Fe, with its content (c_{Fe}) ranging between 0.71 and 1.70 wt % (equivalent to Fe/Mn molar ratios between 0.027 and 0.065). Considering, however, that $La_{0.63}Ca_{0.37}Mn_{1-x}Fe_xO_3$ with $x = 0.08$ still exhibits a relatively sharp FM transition at ~ 170 K and has a low-temperature M_s smaller than that for $x = 0$ by only about 10% (14), the effect of the contaminant Fe is too small to be the primary cause of the spin–glass behavior of the as-milled powders even if all the Fe atoms are incorporated in the $La_{0.7}Ca_{0.3}MnO_z$ phase. (In fact, an analysis of the magnetization curves measured at 300 K ($\gg T_c$ of $La_{0.7}Ca_{0.3}MnO_z$) indicates that no more than half of the contaminant Fe is incorporated in the perovskite lattice.) We thus neglect the effects of the Fe impurities in the following discussions.

[4]Part of Mn^{3+}–Mn^{3+} and Mn^{3+}–Mn^{4+} SE interactions are also negative if static orbital ordering is present (Table 2). Although long-range static orbital ordering, as in $LaMnO_3$, is unlikely in the as-milled powders because of (quasi)cubic symmetry, the possibility of local static orbital ordering cannot be ruled out. In fact, a recent ^{55}Mn NMR study on $LaMnO_{3+\delta}$ and $La_{1-x}Ca_xMnO_3$ (21) has revealed the presence of local AF domains with the sublattice magnetization perpendicular to the external field, characteristic of the A-type AF structure (22), for all v_{Mn} between 3 and 3.23. Uncertainty about the fraction of negative SE interactions for Mn^{3+}–Mn^{3+} and Mn^{3+}–Mn^{4+} pairs, however, does not affect the present qualitative discussion, since Mn^{4+}–Mn^{4+} SE interactions are always negative.

TABLE 2
Superexchange (SE) Interactions between Mn Ions in Perovskite Manganites (31)

Mn^{2+}–Mn^{2+}	$\uparrow\downarrow$	
Mn^{2+}–Mn^{3+}	$\uparrow\downarrow^a$	$\uparrow\uparrow$ & $\uparrow\downarrow^b$
Mn^{2+}–Mn^{4+}	$\uparrow\uparrow$	
Mn^{3+}–Mn^{3+}	$\uparrow\uparrow^a$	$\uparrow\uparrow$ & $\uparrow\downarrow^b$
Mn^{3+}–Mn^{4+}	$\uparrow\uparrow^a$	$\uparrow\uparrow$ & $\uparrow\downarrow^b$
Mn^{4+}–Mn^{4+}	$\uparrow\downarrow$	

[a]Static orbital ordering absent.

[b]Static orbital ordering present. The symbol "$\uparrow\uparrow$ & $\uparrow\downarrow$" indicates anisotropic SE interaction (i.e., the sign depends on the orientation of the occupied e_g orbitals).

Mn^{3+}, Mn^{4+}, and $Mn^{3+/4+}$ and inhomogeneous magnetic structure in $LaMnO_{3+\delta}$ ($0 < \delta \leq 0.15$) have been demonstrated by NMR (21, 24) and neutron diffraction and small-angle neutron scattering (23) studies.

Second, there is additional potential fluctuation near the surface. For one thing, the Mn ions at the surface have various oxygen coordination numbers; for another, the Madelung potential at the surface, set up only by the ions inside the crystal occupying half space, is different from that inside the bulk. Thus, the e_g electrons near the surface, where about a quarter of the Mn ions are located in a 10-nm crystal, are prone to localization even without extrinsic defects, resulting in stronger magnetic disorder. A reduction in M_s with increasing surface area has been observed in $La_{0.7}Ca_{0.3}MnO_3$ and has been explained in terms of this surface effect (25).

The suppression of ferromagnetism, as manifested by a decrease in M_s, with either decreasing or increasing v_{Mn} from 3.3 (inset of Fig. 2c) is qualitatively similar to that observed in other variable-valence systems such as $La_{1-x}Ca_xMnO_3$ (13), $LaMnO_{3+\delta}$ (18,19,23), and $La_{0.67}Ba_{0.33}MnO_z$ (26), and is ascribed to the increasing dominance of antiferromagnetic SE interactions over ferromagnetic DE interactions. A few comments are in order regarding the v_{Mn} dependence of the magnetic properties of the as-milled powders:

1. Recent studies using various kinds of local probe techniques (20,21,23,24,27) have demonstrated that changeover from antiferromagnetism to ferromagnetism, and vice versa, as v_{Mn} is changed in manganites occurs, in general, through changes in the fraction of AF and FM regions, and not through homogeneous spin canting as predicted in an earlier theoretical study (28). Considering the high density of defects, an inhomogeneous magnetic structure almost certainly exists in our as-milled powders; that is, the decrease (increase) in M_s (H_c) with either decreasing or increasing v_{Mn} from 3.3 is due to increases in the fraction of negative SE interactions (see Table 2).

2. As already mentioned, the as-milled powders with $v_{Mn} = 3$ and 3.6 have much larger M_s than bulk $(La,Ca)MnO_3$ samples with the same v_{Mn}. This is ascribed to the high density of defects in the as-milled powders, which prevents orbital and charge ordering. As is well established (22), the "A-type" AF ordering in $LaMnO_3$ requires orbital ordering, while the "CE-type" AF ordering in $La_{1-x}Ca_xMnO_3$ ($x \sim 0.5$) depends on both orbital and charge ordering. The effect of vacancies is analogous to that of Ga ions substituted for Mn in $LaMn_{1-x}Ga_xO_3$, in which suppression of the static cooperative orbital ordering due to Ga substitution induces ferromagnetism despite the unchanged v_{Mn} (29).

3. The powder with $v_{Mn} = 4$, containing only Mn^{4+} ions coupled by negative SE interactions, is regarded as a diluted antiferromagnet. The M versus T curve in Fig. 8 indeed exhibits changes in slope at low temperature with a minimum slope occurring at 23 K. (This feature is seen more clearly in the dM/dT versus T curve.) This is an indication of an AF transition although it is broadened because of the cation vacancies, which dilute SE interactions.

Upon annealing, the electron localization effects responsible for magnetic disorder are alleviated as vacancies are filled and the surface area decreases. Consequently, M_s increases and the temperature dependence of H_c becomes weaker. [The decrease in H_c in the range $T_a > 1000°C$ is ascribed to the increase in D. At $T_a = 1000°C$, D is still so small (~ 40 nm) as to be in the single-domain regime, giving a relatively large $H_c \sim 200$ Oe. At 1450°C, D is large enough (a few micrometers) to allow domain wall formation, and H_c is considerably smaller, < 5 Oe.] M_s increases in a lower T_a range for lower v_{Mn}, since oxygen vacancies, the dominant defects for lower v_{Mn}, are filled in a lower T_a range than cation vacancies, which are the dominant defects for higher v_{Mn}.

CONCLUSIONS

Ultrafine $La_{0.7}Ca_{0.3}MnO_z$ powders have successfully been synthesized by mechanical alloying of La_2O_3, CaO, and a mixture of MnO_2 and Mn_3O_4. Owing to high-energy ball milling, which keeps chemically active fresh surfaces of the reactants in contact with one another through continuous grinding and mixing, the perovskite phase is formed from the constituent oxides at ambient temperature in only 5 h; in a sense, a single-step milling process in mechanical alloying may be regarded as "firing at room temperature" and "regrinding" repeated a large number of times continuously in a vial. It is also found possible to control the oxygen content (z) over a wide range, $2.68 \leq z \leq 3.35$, simply by changing the MnO_2/Mn_3O_4 ratio in the starting mixture. This range of z corresponds to the range of average Mn valence (v_{Mn}) between 2.67 and 4, covering the regions inaccessible by other conventional methods. The present work

thus demonstrates that mechanical alloying is not only an extremely simple economical way of synthesizing mixed-valence perovskite manganites but also an effective tool in producing phases unstable or metastable under normal conditions.

An extensive study of the magnetic properties has revealed spin–glass behavior in the as-milled powders, characterized by reduced spontaneous magnetization, broad ferromagnetic transition, and enhanced coercivity at low temperature. These features, which depend significantly on v_{Mn}, are well understood in terms of magnetic disorder resulting from defects induced by high-energy ball milling and surface effects dominant in small crystals. The changes in the magnetic properties upon annealing, from those of spin–glasses to those of normal soft ferromagnets, are consistent with the disappearance of defects and reduction in the surface area, confirmed by the study of crystal structure and morphology.

REFERENCES

1. A. Urushibara, Y. Moritomo, T. Arima, A. Asamitsu, G. Kido, and Y. Tokura, *Phys. Rev. B* **51,** 14103 (1995).
2. C. W. Searle and S. T. Wang, *Can. J. Phys.* **48,** 2023 (1970).
3. A. Asamitsu, Y. Moritomo, R. Kumai, Y. Tomioka, and Y. Tokura, *Phys. Rev. B* **54,** 1716 (1996).
4. R. J. H. Voorhoeve, J. P. Remeika, P. E. Freeland, and B. T. Matthias, *Science* **177,** 353 (1972).
5. J. J. Heremans, M. Carris, S. Watts, X. Yu, K. H. Dahmen, and S. von Molnár, *J. Appl. Phys.* **81,** 4967 (1997).
6. N. Q. Minh, *J. Am. Ceram. Soc.* **76,** 563 (1993).
7. Z. B. Guo, Y. W. Du, J. S. Zhu, H. Huang, W. P. Ding, and D. Feng. *Phys. Rev. Lett.* **78,** 1142 (1997).
8. R. D. Sánchez, J. Rivas, C. Vázquez-Vázquez, A. López-Quintela, M. T. Causa, M. Tovar, and S. Oseroff, *Appl. Phys. Lett.* **68,** 134 (1996).
9. Z. Jin, W. Tang, J. Zhang, and Y. Du, *J. Magn. Magn. Mater.* **187,** 237 (1998).
10. V. M. Browning, R. M. Stroud, W. W. Fuller-Mora, J. M. Byers, M. S. Osofsky, D. L. Knies, K. S. Grabowski, D. Koller, J. Kim, D. B. Chrisey, and J. S. Horwitz, *J. Appl. Phys.* **83,** 7070 (1998).
11. J. H. Kuo, H. U. Anderson, and D. M. Sparlin, *J. Solid State Chem.* **83,** 52 (1989).
12. J. A. M. Van Roosmalen and E. H. P. Cordfunke, *J. Solid State Chem.* **110,** 106 (1994).
13. G. H. Jonker, *Physica* **22,** 707 (1956).
14. K. H. Ahn, X. W. Wu, K. Liu, and C. L. Chien, *Phys. Rev. B* **54,** 15299 (1996).
15. X. J. Fan, J. H. Zhang, X. G. Li, W. B. Wu, J. Y. Wang, T. J. Lee, and H. C. Ku, *J. Phys.: Condens. Matter* **11,** 3141 (1999).
16. C. Zener, *Phys. Rev.* **82,** 403 (1951).
17. L. Ranno, M. Viret, A. Mari, R. M. Thomas, and J. M. D. Coey, *J. Phys.: Condens. Matter* **8,** L33 (1996).
18. J. Töpfer and J. B. Goodenough, *J. Solid State Chem.* **130,** 117 (1997).
19. M. Muroi and R. Street, *Aust J. Phys.* **52,** 205 (1999).
20. D. Louca, E. L. Brosha, and T. Egami, *Phys. Rev. B* **61,** 1351 (2000).
21. G. Allodi, R. De Renzi, G. Guidi, F. Licci, and M. W. Pieper, *Phys. Rev. B* **56,** 6036 (1997).
22. J. B. Goodenough, *Phys. Rev.* **100,** 564 (1955).
23. C. Ritter, M. R. Ibarra, J. M. De Teresa, P. A. Algarabel, C. Marquina, J. Blasco, J. García, S. Oseroff, and S-W. Cheong, *Phys. Rev. B* **56,** 8902 (1997).
24. Cz. Kapusta and P. C. Riedi, *J. Magn. Magn. Mater.* **196–197,** 446 (1999).
25. M. Muroi, R. Street, and P. G. McCormick, *J. Appl. Phys.* **87,** 3424 (2000).
26. H. L. Ju, J. Gopalakrishnan, J. L. Peng, Qi Li, G. C. Xiong, T. Venkatesan, and R. L. Greene, *Phys. Rev. B* **51,** 6143 (1995).
27. M. Hennion, F. Moussa, J. Rodríguez-Carvajal, L. Pinsard, and A. Revcolevschi, *Phys. Rev. B* **56,** R497 (1997).
28. P. G. de Gennes, *Phys. Rev.* **118,** 141 (1960).
29. J. B. Goodenough, A. Weld, R. J. Arnott, and N. Menyuk, *Phys. Rev.* **124,** 373 (1961).
30. K. Moorjani and J. M. D. Coey, "Magnetic Glasses." Elsevier, Amsterdam, 1984.
31. J. B. Goodenough, "Magnetism and the Chemical Bond." Interscience Publishers, New York, 1963.